Check for updates

*Astronomische Nachrichten*

Astronomische Nachrichten

PROCEEDING

# Can We Draw Conclusions on Supernova Shock Wave Propagation Using Short-Lived Radioactive Isotopes?

Benjamin Wehmeyer[1,2,3,4] | Andrés Yagüe López[5] | Benoit Côté[6] | Maria K. Petö[2,3] | Chiaki Kobayashi[4] | Maria Lugaro[7,8]

[1]Institute of Theoretical Physics, University of Wrocław, Wrocław, Poland | [2]Konkoly Observatory, HUN-REN Research Centre for Astronomy and Earth Sciences, Budapest, Hungary | [3]CSFK, MTA Centre of Excellence, Budapest, Hungary | [4]Centre for Astrophysics Research, University of Hertfordshire, Hatfield, UK | [5]Computer, Computational and Statistical Sciences (CCS) Division, Center for Theoretical Astrophysics, Los Alamos National Laboratory, Los Alamos, New Mexico, USA | [6]Department of Physics and Astronomy, University of Victoria, Victoria, British Columbia, Canada | [7]ELTE Eötvös Loránd University, Institute of Physics, Budapest, Hungary | [8]School of Physics and Astronomy, Monash University, Victoria, Australia

**Correspondence:** Benjamin Wehmeyer (b.wehmeyer@herts.ac.uk)

**Received:** 12 March 2025 | **Accepted:** 13 March 2025

**Funding:** The authors thank Anton Wallner for providing the deep-sea measurement data relevant for this work. We further thank Adrienne Ertel and Jesse Miller for constructive discussion with regard to the PINBALL model at the 2019 JINA-CEE Frontiers meeting. B.C. and B.W. acknowledge support from the National Science Foundation (NSF, USA) under Grant no. PHY-1430152 (JINA Center for the Evolution of the Elements) and Grant no. OISE-1927130 (IReNA). B.W. acknowledges support from the National Center for Science (NCN, Poland) under Grant no. 2022/47/D/ST9/03092. M.K.P. received funding from the European Union's Horizon 2020 research and innovation programme under the Marie Sklodowska-Curie grant agreement No 753276. C.K. acknowledges funding from the UK Science and Technology Facility Council (STFC) through grant ST/R000905/1, & ST/V000632/1. The work was also funded by a Leverhulme Trust Research Project Grant on "Birth of Elements". This work was supported by the ERC Consolidator Grant (Hungary) funding scheme (Project RADIOSTAR, G. A. no. 724560) and by the Lendület Program LP2023-10 of the Hungarian Academy of Sciences. We also thank the COST actions "ChETEC" (G. A. no. 16117) and "ChETEC-INFRA" (G. A. no. 101008324). M.L. was also supported by the NKFIH excellence grant TKP2021-NKTA-64. The work of A.Y.L. was supported by the US Department of Energy through the Los Alamos National Laboratory. Los Alamos National Laboratory is operated by Triad National Security LLC, for the National Nuclear Security Administration of U.S. Department of Energy (Contract No. 89233218CNA000001). Some computations outlined in this paper were performed at the Wroclaw Centre for Scientific Computing and Networking (WCSS).

**Keywords:** astrochemistry | galactic abundances | interstellar medium

## ABSTRACT

We run a three-dimensional Galactic chemical evolution (GCE) model to follow the propagation of $^{53}$Mn (exclusively produced from type Ia supernovae, SNIa), $^{60}$Fe (exclusively produced from core-collapse supernovae, CCSNe), $^{182}$Hf (exclusively produced from intermediate mass stars, IMSs), and $^{244}$Pu (exclusively produced from neutron star mergers, NSMs). By comparing the predictions from our three-dimensional GCE model to recent detections of $^{53}$Mn, $^{60}$Fe, and $^{244}$Pu on the deep-sea floor, we draw conclusions about their propagation in the interstellar medium.

## 1 | Introduction

Introducing short-lived (~Myr) radioactive isotopes (SLRs) in Galactic chemical evolution (e.g., Audouze and Tinsley 1976; Gibson et al. 2003; Kobayashi et al. 2020a; Matteucci and Greggio 1986; Nomoto et al. 2013; Prantzos et al. 2020) further constrains the timing of galactic nucleosynthesis processes: Any given amount of SLRs decays following an exponential law. This means, if we know two of the three characteristic values ((i) produced amount in an astrophysical nucleosynthesis site, (ii) measured/observed amount, (iii) elapsed time between the production and the measurement/observation of the SLR), we can draw conclusions about the third one. This enabled, for example, determining the source, and production sites and conditions for

This is an open access article under the terms of the Creative Commons Attribution License, which permits use, distribution and reproduction in any medium, provided the original work is properly cited.

© 2025 The Author(s). *Astronomische Nachrichten* published by Wiley-VCH GmbH.

various SLRs that influenced the stellar nursery out of which the Sun formed (e.g., Lugaro et al. (2018)). In order to obtain the measured/observed amount at time of the formation of the Solar system, the excess of the daughter isotope of the SLR compared to a reference isotope in meteorites is used.

On the other hand, today's interstellar inventory of certain SLRs can be measured by detecting the $\gamma$-rays emitted along their decay chain (e.g., Diehl 2022). This approach has been used to pinpoint star forming regions in the Galaxy (e.g., Kretschmer et al. 2013), as well as the gas dynamics in the Galaxy (e.g., Krause et al. 2021; Kretschmer et al. 2013).

Here, we make use of a third way to detect SLRs of extraterrestrial origin: Some deep-sea Earth crust samples contain some interstellar $^{53}$Mn, $^{60}$Fe, and $^{244}$Pu isotopes (e.g., Korschinek et al. (2020); Wallner et al. (2015, 2016, 2021)). These SLRs of interstellar origin accumulated on the bottom of the ocean over several My. Taking probes from the Earth's crust, and analyzing slices of these probes permits to draw conclusions about the interstellar densities of these SLRs over the course of the last 12 My. (e.g., Korschinek et al. (2020); Wallner et al. (2015, 2016, 2021)). In this work, we use these derived densities in our cubic three-dimensional GCE model Wehmeyer et al. (2019); Wehmeyer et al. (2015) to draw conclusions about the CCSN explosion shock wave propagation properties. We further predict the presence of a fourth key SLR, $^{182}$Hf, in these samples, and show its predicted densities in the interstellar medium over the course of the same time span as covered by the deep-sea probes.

## 2 | Model

We used the three-dimensional GCE model described in Wehmeyer et al. (2019, 2015). The model simulates a periodic boundary condition, three-dimensional box with an edge length of 2 kpc. The box is divided into sub-cubes with an edge length of 50 pc. Starting from this model, we added a radioactive decay module, and follow the evolution of the four SLRs, $^{53}$Mn, $^{60}$Fe, $^{182}$Hf, and $^{244}$Pu (Wehmeyer et al. 2023). The time step size is 1 Myr, during which the chemical evolution calculations are performed. We provide an overview of the calculations below:

1. *Gas infall*. Gas with primordial composition is inserted into the simulation volume, following an analytic formula that permits an early rise, and a late exponential decrease of the insertion.
2. *Star formation*. A Schmidt law (exponent $\alpha = 1.5$, Kennicutt (Kennicutt and Robert 1998); Larson (1991); Schmidt (1959)) is used to determine the number of stars created in the time step. From the number of newly born stars, a Salpeter initial mass function (Salpeter 1955) with a slope of −2.35 is used to determine the mass of the newly born stars within the range $0.1\,M_\odot \leq m \leq 50\,M_\odot$. The Geneva group's (Charbonnel et al. 1993; Schaerer et al. 1993a, 1993b) equation

$$\log(t) = (3.79 + 0.24Z) - (3.10 + 0.35Z)\log(M) + (0.74 + 0.11Z)\log^2(M), \quad (1)$$

is used to calculate the life expectation for each newly born star. (t is the expected lifetime of the star in Myr, Z is the metallicity, and M the mass in Solar masses).

3. *Stellar deaths*. During every time step, there is a number of stars which have reached the end of their life expectancy. For these stars, their death will be treated as outlined in Sections 2.1 and 2.2 below.
4. *Double star systems*. The Galaxy hosts many double- or triple star systems (e.g., Duchêne and Kraus (2013)). Depending on their initial mass, these systems have a chance to later end up in a thermonuclear supernova explosion (SNIa, for intermediate mass stars), or a neutron star merger (NSM, in the case of massive stars). We take this into account by introducing two probability factors, representing the probability of such a system to later undergo such an event, $P_{SNIa} = 6 \cdot 10^{-3}$ as the fraction of all newly born IMSs to later undergo SNIa, $P_{NSM} = 0.04$) representing the fraction of all newly born HMSs to later end up in a NSM. From the number for NSMs ($P_{NSM}$), we can find the cosmic gravitational wave emission rate (see Côté et al. (2017) for details) $\approx$ 1800 Gpc$^{-3}$ yr.$^{-1}$, which is a bit larger than the LIGO/Virgo rate of (810 Gpc$^{-3}$ yr.$^{-1}$ Abbott et al. (2021)). The nucleosynthesis ejecta of the two sites are disussed in Sections 2.3 and 2.4 below.
5. At every time step, the gas content and the SLR abundance in every cell are stored.

### 2.1 | Intermediate Mass Stars

IMSs do not significantly contribute to the nucleosynthesis of the ISM. Their main task is to lock up gas during their lifetime, and then re-eject parts of the gas, together with $^{182}$Hf (with yields from table S1 in the Supporting Information of Lugaro et al. 2014) at the end of their lifetime.

### 2.2 | Massive Stars

At the end of their life, HMSs die in a CCSN explosion under the ejection of elements as in Nomoto et al. (1997); Thielemann et al. (1996), together with $^{60}$Fe according to yields in Table 3 in Limongi and Chieffi (2006). To account for the effect of hypernovae (e.g., Nomoto et al. 2013, 2004) and the propagation of the ejecta post-supernova (Feige et al. 2017; Fry et al. 2018), we consider different models, as outlined in Section 2.5.

### 2.3 | Thermonuclear Supernovae

Once this longer-lived IMS in a double star system has reached the end of its lifetime, the system ends as SNIa. The system ejects nuclei according to the yields in table 3 in Iwamoto et al. (1999) (model CDD2), as well as $10^{-4}$ $M_\odot$ of $^{53}$Mn, in agreement with (Kobayashi et al. 2020b; Seitenzahl et al. 2013). The kinetic energy ejected in the event will sweep up $5 \times 10^4 M_\odot$ of ISM.



15213994, 2025, 3-4, Downloaded from https://onlinelibrary.wiley.com/doi/10.1002/asna.70002 by Michigan State University, Wiley Online Library on [03/11/2025]. See the Terms and Conditions (https://onlinelibrary.wiley.com/terms-and-conditions) on Wiley Online Library for rules of use; OA articles are governed by the applicable Creative Commons License

## 2.4 | Neutron Star Mergers

Once the two NS were produced in two preceding CCSNe, they orbit each other under the emission of gravitational waves for a coalescence time ($t_{coal} = 10^8$ years in our simulation), until they merge. Upon merging, the NSM ejects $10^{-8}$ $M_{\odot}$ of $^{244}$Pu (in agreement with Eichler et al. (2015)), assuming a total ejecta mass of $10^{-2}$ $M_{\odot}$ and a mass fraction of $X_{244} = 10^{-6}$. The ejecta will then sweep up the surrounding ISM and pollute it with $^{244}$Pu.

## 2.5 | Supernova Ejecta Dynamics

To account for the effect of hypernovae (e.g., Nomoto et al. 2013, 2004), and the effect of a varied CCSN bubble remnant geometry due to, e.g., magnetic fields, or hydrodynamical effects (e.g., Feige et al. 2017; Fry et al. 2018), we set up four different scenarios (Table 1) to study the implications assuming differenct CCSN ejecta dynamics with the ISM:

1. *Standard case*. All CCSNe explode with a kinetic energy of $10^{51}$ erg, and which corresponds to $5 \cdot 10^4$ $M_{\odot}$ of swept-up ISM. All ejected elements and SLRs are deposited the blast wave shell.
2. *Increased explosion energy case (hypernova model, HN)*. To estimate the contribution of hypernovae, we increase the explosion energy of all CCSNe to sweep up $2 \cdot 10^5$ $M_{\odot}$ of ISM. As in the standard case, The remnant geometry is the same as in the standard case, all ejected elements and SLRs are deposited the blast wave shell.
3. *Modified geometry case (PINBALL)*. To estimate the impact of magnetic field effects, we use a "pinball model"-style remnant geometry (Fry et al. 2018). Here, the magnetic field inside the remnant reflects the SLRs backwards, so they behave like a pinball inside of the remnant, which results in a much more well-distributed remnant bubble. As in the standard case, all CCSNe explode with an energy of $10^{51}$ erg, but 1% of the swept-up SLRs stay within the explosion bubble.
4. *Combination of increased explosion energy and modified geometry (HN PINBALL)*. The combination of models HN and PINBALL. All CCSNe pollute $2 \cdot 10^5$ $M_{\odot}$ of ISM, as in the HN model, and 1% of the swept-up ISM stay inside the explosion bubble as in the PINBALL model.

In the model, we deliberately chose a time step size of 1 Myr because this allows us to simplify all thermo- and hydrodynamic processes (as considered in, e.g., Feige et al. 2017) into one single value, the swept-up mass. This choice further enables us to omit all the microphysics regarding star formation processes, as we can simply use the statistical Schmidt law.

**TABLE 1** | Overview over the different models.

| Model name | ISM polluted | Remnant geometry |
|---|---|---|
| Standard | $5 \cdot 10^4$ $M_{\odot}$ | Standard |
| HN | $2 \cdot 10^5$ $M_{\odot}$ | Standard |
| PINBALL | $5 \cdot 10^4$ $M_{\odot}$ | PINBALL model |
| HN PINBALL | $2 \cdot 10^5$ $M_{\odot}$ | PINBALL model |

## 3 | Results

Figure 1 shows a zoom-in of the evolution of the abundances of the four SLRs, close to current day, for the different models described in Section 2.5. Also, we added the (time-shifted) deep-sea detections from Wallner et al. (2016), Korschinek et al. (2020) and Wallner et al. (2021) to the Figure. Since the statistical evolution of the SLR in all cells (gray scales/black) does not tell us much about their correspondence to the deep-sea detections, we also added the evolution of the single, best fitting sub-cell of the entire simulation volume to the Figure (green line).

To better be able to draw better conclusions, we introduced a time-shift factor $\Delta t$, as well as a vertical shift factor $\lambda$ for all isotope detections, since it is more interesting to fit the shape of the detection curves, rather than the actual values. The values for these factors for each model are listed in Table 2.

In the top left panel of Figure 1, we can see the radioactive decay of all four isotopes around 13335 Myr.

But, the more striking feature of that plot is the violent upward and downward movements that often coincides in more of the SLRs. This effect originates in the Sedov-Taylor-like expansion pattern of CCSN shock waves, as SLRs are pushed violently throughout the simulation volume. The sudden decreases in SLRs can be explained by CCSN shock waves traveling through and emptying the best-fitting sub-cell (green line). The sudden increases occur if such a CCSN shock wave is stopped right in the location of the best-fitting sub-cell (green line) and thus enhancing that sub-cell with all the swept-up material.

This effect can be observed in all four panels of Figure 1. The difference, though, is the intensity of this effect:

In the top right panel of Figure 1 (HN model), the fluctuations are much more prominent. This comes from the fact that the CCSN explosions are much more violent than in the standard model, and thus push around the ISM and SLRs much more violently, which leads to a more abrupt behavior of the SLRs in the best-fitting sub-cell (green line).

For the PINBALL model case (bottom left panel of Figure 1), we can see that the evolution of the best-fitting sub-cell (green line) is more variable than in the top left panel of Figure 1. This is because more cells are affected by every CCSN explosion shock wave, since more material is left behind, instead of depositing all the material (and SLRs) only on the shell. More cells affected by every CCSN means more sub-cells affected per time step, which in turn means that the abundance in the best-fitting sub-cell (green line) is affected more often in any given time interval.

The evolution of the SLRs in the best-fitting sub-cell (green line) oscillates strongest of all models in the lower right panel of Figure 1 (HN PINBALL model). In this model, not only the radii of the CCSN explosion shock waves are highest (as high as in the



15213994, 2025, 3-4, Downloaded from https://onlinelibrary.wiley.com/doi/10.1002/asna.70002 by Michigan State University, Wiley Online Library on [03/11/2025]. See the Terms and Conditions (https://onlinelibrary.wiley.com/terms-and-conditions) on Wiley Online Library for rules of use; OA articles are governed by the applicable Creative Commons License

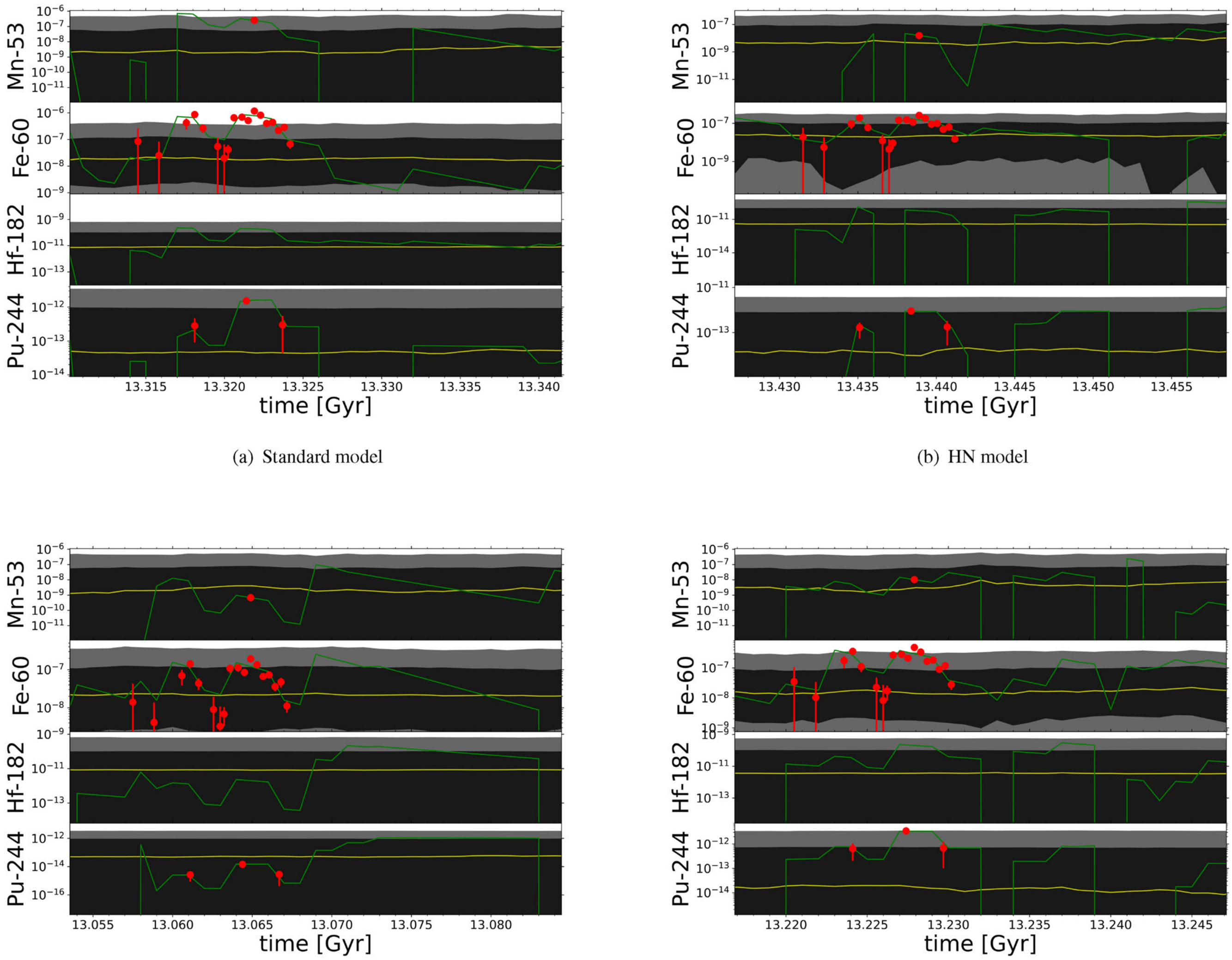


(a) Standard model

(b) HN model

(c) PINBALL model

(d) HN PINBALL model

**FIGURE 1** | Zoomed-in evolution of the four focus SLRs, ±15 Myr around the respective $\Delta t$. Inferred ISM densities for $^{53}$Mn, $^{60}$Fe, and $^{244}$Pu, are also shown as red symbols with error bars (shifted by factors $\lambda$ and $\Delta t$). The evolution of the best-fitting sub-cell is represented in a green line.

HN model) due to the higher explosion energies, but also the pinball remnant geometry leads to more sub-cells within the shock wave remnant to be polluted. The combination of these two factors leads to most sub-cells affected of all the four models per time step, which in turn means that the best-fitting sub-cell (green line) is most affected of all models during any given time interval. Overall, it is possible to find a best-fitting sub-cell (green line) that reasonably agrees with the deep-sea detections in all four models. To be able to judge how good the agreement is, we introduce a "goodness factor" $S$, the mean squared distance of the logarithm of the abundances to the actual deep-sea detections[1], with $S$ given by

$$S = \frac{1}{N} \sum \left( \frac{\ln R(t_i) - \ln Y_i}{\ln(Y_i + E_i) - \ln Y_i} \right)^2. \quad (2)$$

where $R(t_i)$ is the abundance of the model at time $t_i$, and $Y_i$ and $E_i$ the deep-sea measurement and uncertainties at time $t_i$. For the standard model, the S-factor is 4.07, for the HN model, the S-factor is 4.15, for the PINBALL model, the S factor is 4.24, and the HN PINBALL model, it is 4.23. This means, that the standard model best fits the deep-sea detections.

**TABLE 2** | Vertical ($\lambda$) and time-shift ($\Delta t$) factors for the ISM densities of the deep-sea detection of the three detected isotopes.

| Model name | $\lambda_{53_{Mn}}$ | $\lambda_{60_{Fe}}$ | $\lambda_{244_{Pu}}$ | $\Delta t$ (Myr) |
|---|---|---|---|---|
| Standard | 0.211 | 134 | 16.5 | 174.63 |
| HN | 0.125 | 29.7 | 1.01 | 57.63 |
| PINBALL | 0.002 | 22.1 | 0.0439 | 431.63 |
| HN PINBALL | 0.476 | 55.2 | 0.669 | 268.63 |

## 4 | Conclusions and Discussion

We have presented a three-dimensional model to follow the evolution of four focus SLRs, $^{53}$Mn, $^{60}$Fe, $^{182}$Hf, and $^{244}$Pu. We have



15213994, 2025, 3-4, Downloaded from https://onlinelibrary.wiley.com/doi/10.1002/asna.70002 by Michigan State University, Wiley Online Library on [03/11/2025]. See the Terms and Conditions (https://onlinelibrary.wiley.com/terms-and-conditions) on Wiley Online Library for rules of use; OA articles are governed by the applicable Creative Commons License

compared the evolution of these SLRs to their detections in different layers in the deep-sea deposits, corresponding to their infall on Earth at different times. We conclude that our standard model (all CCSNe explode with a kinetic energy of $10^{51}$ erg, their ejecta distributed in a non-pinball-style pattern, that is, exclusively homogeneously distributed on the shock wave shell) statistically best reproduces the shape of the detections. Further investigations are necessary to draw firmer conclusions about the propagation mechanism of the SLRs.

Future detections of live radioisotopes of interstellar origin in the deep-sea floor (e.g., Wang et al. 2021a, 2021b) will further constrain the mechanism and properties of the associated nucleosynthesis sites. Further, real magnetic field calculations and their implications should be applied, as well as proper thermodynamic treatment (as done in, e.g., Feige et al. 2017).


## Acknowledgments

The authors thank Anton Wallner for providing the deep-sea measurement data relevant for this work. We further thank Adrienne Ertel and Jesse Miller for constructive discussion with regard to the PINBALL model at the 2019 JINA-CEE Frontiers meeting. B.C. and B.W. acknowledge support from the National Science Foundation (NSF, USA) under Grant no. PHY-1430152 (JINA Center for the Evolution of the Elements) and Grant no. OISE-1927130 (IReNA). B.W. acknowledges support from the National Center for Science (NCN, Poland) under Grant no. 2022/47/D/ST9/03092. M.K.P. received funding from the European Union's Horizon 2020 research and innovation programme under the Marie Sklodowska-Curie grant agreement No 753276. C.K. acknowledges funding from the UK Science and Technology Facility Council (STFC) through grant ST/R000905/1, & ST/V000632/1. The work was also funded by a Leverhulme Trust Research Project Grant on "Birth of Elements". This work was supported by the ERC Consolidator Grant (Hungary) funding scheme (Project RADIOSTAR, G. A. no. 724560) and by the Lendület Program LP2023-10 of the Hungarian Academy of Sciences. We also thank the COST actions "ChETEC" (G. A. no. 16117) and "ChETEC-INFRA" (G. A. no. 101008324). M.L. was also supported by the NKFIH excellence grant TKP2021-NKTA-64. The work of A.Y.L. was supported by the US Department of Energy through the Los Alamos National Laboratory. Los Alamos National Laboratory is operated by Triad National Security LLC, for the National Nuclear Security Administration of U.S. Department of Energy (Contract No. 89233218CNA000001). Some computations outlined in this paper were performed at the Wroclaw Centre for Scientific Computing and Networking (WCSS).


## Conflicts of Interest

The authors declare no conflicts of interest.

## Endnotes

[1] Assuming the abundances follow a normal distribution with $\sigma$ equal to the uncertainty.

## References


Abbott, R., T. D. Abbott, S. Abraham, et al. 2021. "Population Properties of Compact Objects from the Second LIGO-Virgo Gravitational-Wave Transient Catalog." *Astrophysical Journal* 913, no. 1: L7.

Audouze, J., and B. M. Tinsley. 1976. "Chemical Evolution of Galaxies." *Annual Review of Astronomy and Astrophysics* 14: 43–79.

Charbonnel, C., G. Meynet, A. Maeder, G. Schaller, and D. Schaerer. 1993. "Grids of stellar models. III. From 0.8 to 120 Msolar at Z=0.004." *Astronomy & Astrophysics* 101: 415.

Côté, B., K. Belczynski, C. L. Fryer, et al. 2017. "Advanced LIGO Constraints on Neutron Star Mergers and r-process Sites." *Astrophysical Journal* 836, no. 2: 230.

Diehl, R. 2022. "Gamma-Ray Observations of Cosmic Nuclei." *European Physical Journal Web of Conferences* 260: 10001.

Duchêne, G., and A. Kraus. 2013. "Stellar Multiplicity." *Annual Review of Astronomy and Astrophysics* 51, no. 1: 269–310.

Eichler, M., A. Arcones, A. Kelic, et al. 2015. "The Role of Fission in Neutron Star Mergers and Its Impact on the r-Process Peaks." *Astrophysical Journal* 808, no. 1: 30.

Feige, J., D. Breitschwerdt, A. Wallner, et al. 2017. "The Link Between the Local Bubble and Radioisotopic Signatures on Earth." In *14th International Symposium on Nuclei in the Cosmos (NIC2016)*, edited by S. Kubono, T. Kajino, S. Nishimura, et al., 10304. The Physical Society of Japan.

Fry, B. J., B. D. Fields, and J. R. Ellis. 2018. "*arXiv e-prints*, arXiv:1801.06859".

Gibson, B. K., Y. Fenner, A. Renda, D. Kawata, and H.-C. Lee. 2003. *Publications of the Astronomical Society of Australia* 20, no. 4: 401–415. Galactic Chemical Evolution.

Iwamoto, K., F. Brachwitz, K. Nomoto, et al. 1999. "Nucleosynthesis in Chandrasekhar Mass Models for Type Ia Supernovae and Constraints on Progenitor Systems and Burning-Front Propagation." *Astrophysical Journal Supplement* 125, no. 2: 439–462.

Kennicutt, J., and C. Robert. 1998. "The Global Schmidt Law in Star-forming Galaxies." *Astrophysical Journal* 498, no. 2: 541–552.

Kobayashi, C., A. I. Karakas, and M. Lugaro. 2020a. "The Origin of Elements from Carbon to Uranium." *Astrophysical Journal* 900, no. 2: 179.

Kobayashi, C., S.-C. Leung, and K. Nomoto. 2020b. "New Type Ia Supernova Yields and the Manganese and Nickel Problems in the Milky Way and Dwarf Spheroidal Galaxies." *Astrophysical Journal* 895, no. 2: 138.

Korschinek, G., T. Faestermann, M. Poutivtsev, et al. 2020. "Supernova-Produced Mn-53 on Earth." *Physical Review Letters* 125, no. 3: 031101.

Krause, M. G. H., D. Rodgers-Lee, J. E. Dale, R. Diehl, and C. Kobayashi. 2021. "Galactic Al-26 Traces Metal Loss through Hot Chimneys." *Monthly Notices of the Royal Astronomical Society* 501, no. 1: 210–218.

Kretschmer, K., R. Diehl, M. Krause, et al. 2013. "Kinematics of Massive Star Ejecta in the Milky Way as traced by Al-26." *Astronomy & Astrophysics* 559: A99.

Larson, R. B. 1991. "Galactic Evolution." In *Frontiers of Stellar Evolution*, edited by D. L. Lambert, vol. 20, 571. Astronomical Society of the Pacific.

Limongi, M., and A. Chieffi. 2006. "The Nucleosynthesis of Al-26 and Fe-60 in Solar Metallicity Stars Extending in Mass from 11 to 120 Msolar: The Hydrostatic and Explosive Contributions." *Astrophysical Journal* 647, no. 1: 483–500.

Lugaro, M., A. Heger, D. Osrin, et al. 2014. "Stellar Origin of the Hf-182 Cosmochronometer and the Presolar History of Solar System Matter." *Science* 345, no. 6197: 650–653.

Lugaro, M., U. Ott, and Á. Kereszturi. 2018. "Radioactive Nuclei from Cosmochronology to Habitability." *Progress in Particle and Nuclear Physics* 102: 1–47.

Matteucci, F., and L. Greggio. 1986. "Relative Roles of Type I and II Supernovae in the Chemical Enrichment of the Interstellar Gas." *Astronomy & Astrophysics* 154, no. 1–2: 279–287.

Nomoto, K., M. Hashimoto, T. Tsujimoto, et al. 1997. "Nucleosynthesis in Type II Supernovae." *Nuclear Physics A* 616: 79–90.




15213994, 2025, 3-4, Downloaded from https://onlinelibrary.wiley.com/doi/10.1002/asna.70002 by Michigan State University, Wiley Online Library on [03/11/2025]. See the Terms and Conditions (https://onlinelibrary.wiley.com/terms-and-conditions) on Wiley Online Library for rules of use; OA articles are governed by the applicable Creative Commons License

Nomoto, K., C. Kobayashi, and N. Tominaga. 2013. "Nucleosynthesis in Stars and the Chemical Enrichment of Galaxies." *Annual Review of Astronomy and Astrophysics* 51, no. 1: 457–509.

Nomoto, K., K. Maeda, P. A. Mazzali, H. Umeda, J. Deng, and K. Iwamoto. 2004. "Hypernovae and Other Black-Hole-Forming Supernovae." In *Astrophysics and Space Science Library*, edited by C. L. Fryer, vol. 302, 277–325. Springer.

Prantzos, N., C. Abia, S. Cristallo, M. Limongi, and A. Chieffi. 2020. "Chemical Evolution with Rotating Massive Star Yields II. A New Assessment of the Solar s- and r- process Components." *Monthly Notices of the Royal Astronomical Society* 491, no. 2: 1832–1850.

Salpeter, E. E. 1955. "The Luminosity Function and Stellar Evolution." *Astrophysical Journal* 121: 161.

Schaerer, D., C. Charbonnel, G. Meynet, A. Maeder, and G. Schaller. 1993a. "Grids of Stellar Models. IV. From 0.8 to 120 Solar Masses at Z=0.040." *Astronomy & Astrophysics* 102: 339.

Schaerer, D., G. Meynet, A. Maeder, and G. Schaller. 1993b. "Grids of stellar models. II. From 0.8 to 120 solar masses at Z=0.008." *Astronomy & Astrophysics* 98: 523.

Schmidt, M. 1959. "The Rate of Star Formation." *Astrophysical Journal* 129: 243.

Seitenzahl, I. R., F. Ciaraldi-Schoolmann, F. K. Röpke, et al. 2013. "Three-Dimensional Delayed-Detonation Models with Nucleosynthesis for Type La Supernovae." *Monthly Notices of the Royal Astronomical Society* 429, no. 2: 1156–1172.

Thielemann, F.-K., K. Nomoto, and M.-A. Hashimoto. 1996. "Core-Collapse Supernovae and Their Ejecta." *Astrophysical Journal* 460: 408.

Wallner, A., T. Faestermann, J. Feige, et al. 2015. "Abundance of Live Pu-244 in Deep-Sea Reservoirs on Earth Points to Rarity of Actinide Nucleosynthesis." *Nature Communications* 6: 5956.

Wallner, A., J. Feige, N. Kinoshita, et al. 2016. "Recent near-Earth supernovae probed by global deposition of interstellar radioactive Fe-60." *Nature* 532, no. 7597: 69–72.

Wallner, A., M. B. Froehlich, M. A. C. Hotchkis, et al. 2021. "Fe-60 and Pu-244 deposited on Earth constrain the r-process yields of recent nearby supernovae." *Science* 372, no. 6543: 742–745.

Wang, X., A. Clark, J. Ellis, et al. 2021a. "R-Process Radioisotopes From Near-Earth Supernovae and Kilonovae." In *APS Division of Nuclear Physics Meeting Abstracts*, vol. 2021, MD.008. American Physical Society.

Wang, X., A. M. Clark, J. Ellis, et al. 2021b. *arXiv e-prints*, arXiv:2112.09607.

Wehmeyer, B., C. Fröhlich, B. Côté, M. Pignatari, and F. K. Thielemann. 2019. "Using Failed Supernovae to Constrain the Galactic R-Process Element Production." *Monthly Notices of the Royal Astronomical Society* 487, no. 2: 1745–1753.

Wehmeyer, B., A. Y. López, B. Côté, K. Pető, C. Kobayashi, and M. Lugaro. 2023. "Inhomogeneous Enrichment of Radioactive Nuclei in the Galaxy: Deposition of Live Mn-53, Fe-60, Hf-182, and Pu-244 into Deep-sea Archives. Surfing the Wave?" *Astrophysical Journal* 944, no. 2: 121.

Wehmeyer, B., M. Pignatari, and F. K. Thielemann. 2015. "Galactic Evolution of Rapid Neutron Capture Process Abundances: The Inhomogeneous Approach." *Monthly Notices of the Royal Astronomical Society* 452, no. 2: 1970–1981.



15213994, 2025, 3-4, Downloaded from https://onlinelibrary.wiley.com/doi/10.1002/asna.70002 by Michigan State University, Wiley Online Library on [03/11/2025]. See the Terms and Conditions (https://onlinelibrary.wiley.com/terms-and-conditions) on Wiley Online Library for rules of use; OA articles are governed by the applicable Creative Commons License